



# Reverse Transcription Recombinase Polymerase Amplification Coupled with CRISPR-Cas12a for Facile and Highly Sensitive Colorimetric SARS-CoV-2 Detection

Wei S. Zhang,<sup>||</sup> Jianbin Pan,<sup>||</sup> Feng Li, Min Zhu, Mengting Xu, Hongyan Zhu, Yanyan Yu,<sup>\*</sup> and Gaoxing Su<sup>\*</sup>



Cite This: *Anal. Chem.* 2021, 93, 4126–4133



Read Online

ACCESS |



Metrics & More

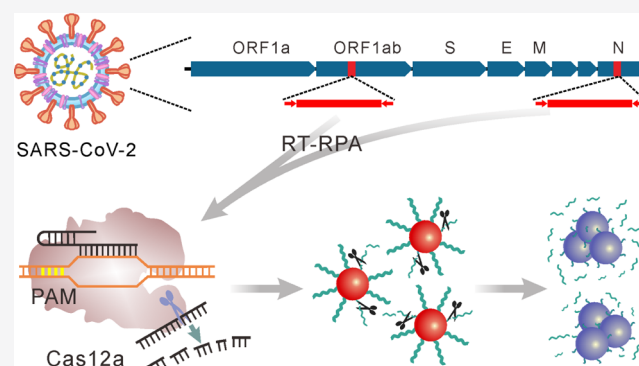


Article Recommendations



Supporting Information

**ABSTRACT:** The outbreak of the pandemic caused by the severe acute respiratory syndrome coronavirus-2 (SARS-CoV-2) calls for an urgent unmet need for developing a facile and cost-effective detection method. The requirement of well-trained personnel and sophisticated instrument of current primary mean (reverse transcription polymerase chain reaction, RT-PCR) may hinder the practical application worldwide. In this regard, a reverse transcription recombinase polymerase amplification (RT-RPA) coupled with CRISPR-Cas12a colorimetric assay is proposed for the SARS-CoV-2 detection. The methodology we have described herein utilizes DNA-modified gold nanoparticles (AuNPs) as a universal colorimetric readout and can specifically target ORF1ab and N regions of the SARS-CoV-2 genome. After the virus genome is amplified through RT-RPA, the resulting abundant dsDNA will bind and activate Cas12a. Under trans-cleavage degradation, the capped DNA substrate will be hydrolyzed gradually from AuNPs, demonstrating a change in the surface plasmon resonance (SPR), which can be facially monitored by UV–vis absorbance spectroscopy and naked eye observation. The high amplification efficiency from RT-RPA and Cas12a trans-cleavage process bring the sensitivity of our method to 1 copy of viral genome sequence per test. Notably, under the dual variations inspecting from the isothermal amplification and Cas12a activation process, the false positive events from other beta coronavirus members can be effectively avoided and thus significantly improve the specificity. Furthermore, the reliability of this colorimetric assay is validated by standard clinical samples from the hospital laboratory department. Through integration of the inherently high sensitivity and specificity from an RPA-coupled Cas12a system with the intrinsic simplicity of AuNP-based colorimetric assay, our method increases the practical testing availability of SARS-CoV-2.



## INTRODUCTION

Severe acute respiratory syndrome coronavirus-2 (SARS-CoV-2), the pathogen causing COVID-19, has caused worldwide pandemic, resulting in more than 30 million reported cases in over 200 countries.<sup>1–3</sup> Considering the undetected mild or asymptomatic cases, the total number of COVID-19 is underestimated. Although the development of therapeutics and vaccines is underway, the diagnosis still plays a vital role in infection prevention and control of epidemic.<sup>4,5</sup> As a single-stranded RNA (ssRNA) virus, SARS-CoV-2 contains 29,903 nucleotide (nt) RNA genomes.<sup>2</sup> Based on the identification and sequence of the SARS-CoV-2 genome, reverse transcription polymerase chain reaction (RT-PCR) techniques developed rapidly and have become the primary means for SARS-CoV-2 detection.<sup>6,7</sup> The gene encoding for envelope (E), nucleocapsid (N), membrane (M), spike (S) proteins and the open reading frame 1ab (ORF1ab) have been selected as RT-PCR targets by different countries.<sup>8</sup> During a typical RT-

PCR assay process, the viral RNA is converted to a complementary DNA (cDNA) before being exponentially amplified through temperature cycling.<sup>9</sup> Despite the wide use, several limitations remain to be improved. The high false negative rate derived from the sampling and operation procedures call for improvements. In addition, the requirement of well-trained personnel and expensive laboratory instrument may hinder practical applications outside well-equipped areas.<sup>10,11</sup> Therefore, there is an urgent unmet need for

Received: January 3, 2021

Accepted: January 29, 2021

Published: February 11, 2021



developing a simple, rapid, cost-effective, and specific test for COVID-19.

In comparison with RT-PCR, the isothermal amplification technique without the requirement for a thermal cycler is more ideal for applications.<sup>12</sup> Typically, the loop-mediated isothermal amplification (LAMP) and recombinase polymerase amplification (RPA) with similar sensitivity to PCR, which can be operated at a single temperature, have been exploited for nucleic acid detection.<sup>13,14</sup> Especially, by incorporation with clustered regularly interspaced short palindromic repeats (CRISPR) technology, the isothermal amplification approaches have been successfully utilized for SARS-CoV-2 detection.<sup>15</sup> As an adaptive immune system, the CRISPR/Cas system uses RNA-guided nucleases to cleave foreign genetic elements. It has been reported that Cas9, Cas12a, Cas13, and Cas14 all show nonspecific trans-cleavage activity after the site-specific binding of target nucleic acids, thus endowing the CRISPR/Cas system with great potential to develop accurate and portable diagnostic tools.<sup>16–19</sup> Through integration of RT-LAMP with CRISPR, Broughton et al. proposed a CRISPR-Cas12-based lateral flow assay for SARS-CoV-2 detection, albeit with reduced sensitivity compared with PCR assay.<sup>20</sup> As an efficient method, RPA can be performed at 37–42 °C, endowing RPA better compatibility with CRISPR technology in terms of the optimal reaction temperature. SHERLOCK, developed by Zhang et al., employed RPA for amplification and Cas13 collateral cutting ability for signal reporting.<sup>21</sup> Meanwhile, SHERLOCK was also demonstrated for SARS-CoV-2 detection recently.<sup>22</sup> As Cas13 selectively responds to RNA, they use RT-RPA to amplify the virus RNA to dsDNA and then transcribe dsDNA to single-strand RNA for Cas13 activation.<sup>23,24</sup> Cas12a, on the other hand, after RNA-guided DNA binding, will exhibit site-specific dsDNA cutting and nonspecific ssDNA trans-cleavage ability. Thus, the DNA-responsive Cas12a may provide more predominance for SARS-CoV-2 in the aspect of operation cost and detection robustness.<sup>25–27</sup> However, most of the CRISPR-based strategies rely on expensive dual-labeled fluorescence reporters and fluorescence detection equipment.

Colorimetric assay based on gold nanoparticles (AuNPs) appeared to be a facial and cost-effective method that is well amenable for the clinical sample detection.<sup>28–30</sup> The exceptional optical properties of AuNPs such as high extinction coefficient, localized surface plasmon resonance (SPR), and inherent photostability have been utilized in abundant colorimetric-based biosensing methods for small molecules and proteins.<sup>31–35</sup> Notably, the optical properties exhibited by the AuNP dispersion state can easily be identified with naked eyes or UV–vis absorbance spectroscopy. Inspired by the pioneering work of Mirkin et al., the colorimetric detection through recruiting nucleic acid-labeled AuNPs has been successfully applied to DNA or RNA detection.<sup>36–39</sup> Nevertheless, to circumvent the sluggish response and poor detection limit constraints, nonenzyme and enzyme-assisted signal amplification methods are always integrated with the colorimetric method.<sup>40–43</sup>

Herein, an isothermal amplification method (RT-RPA)-coupled CRISPR-Cas12a colorimetric assay is proposed for SARS-CoV-2 genome detection. The RT-RPA process will achieve exponential amplification in a short time under an isothermal temperature. Meanwhile, the binding-induced cleavage property of Cas12a will inspect the accuracy of the amplification copies and respond specifically toward the target

sequence.<sup>9</sup> In this way, the RPA-coupled Cas12a will ensure the analytical performance in terms of specificity and selectivity. Furthermore, the AuNP-based colorimetric detection will maintain the exclusive simplicity of the strategy. The methodology we described herein can specifically target an ORF1ab and N regions of the SARS-CoV-2 genome mediated by two pairs of primers and corresponding crRNA. The ssDNA capped AuNPs act as universal results readout process and will be able to accommodate different target detection. The aggregation of AuNPs caused by the SARS-CoV-2 genome can be monitored by UV–vis absorbance spectroscopy as well as naked eye observation. Severe acute respiratory syndrome (SARS-CoV) and Middle East respiratory syndrome (MERS-CoV) sequences as well as clinic standard SARS-CoV-2 genome samples are tested to verify the reliability of the method. Benefiting from the intrinsic merits from the RT-RPA-coupled Cas12a reaction and colorimetric assay, the detection platform we proposed ensured great feasibility and potential for COVID-19 diagnosis even outside the well-equipped regions.

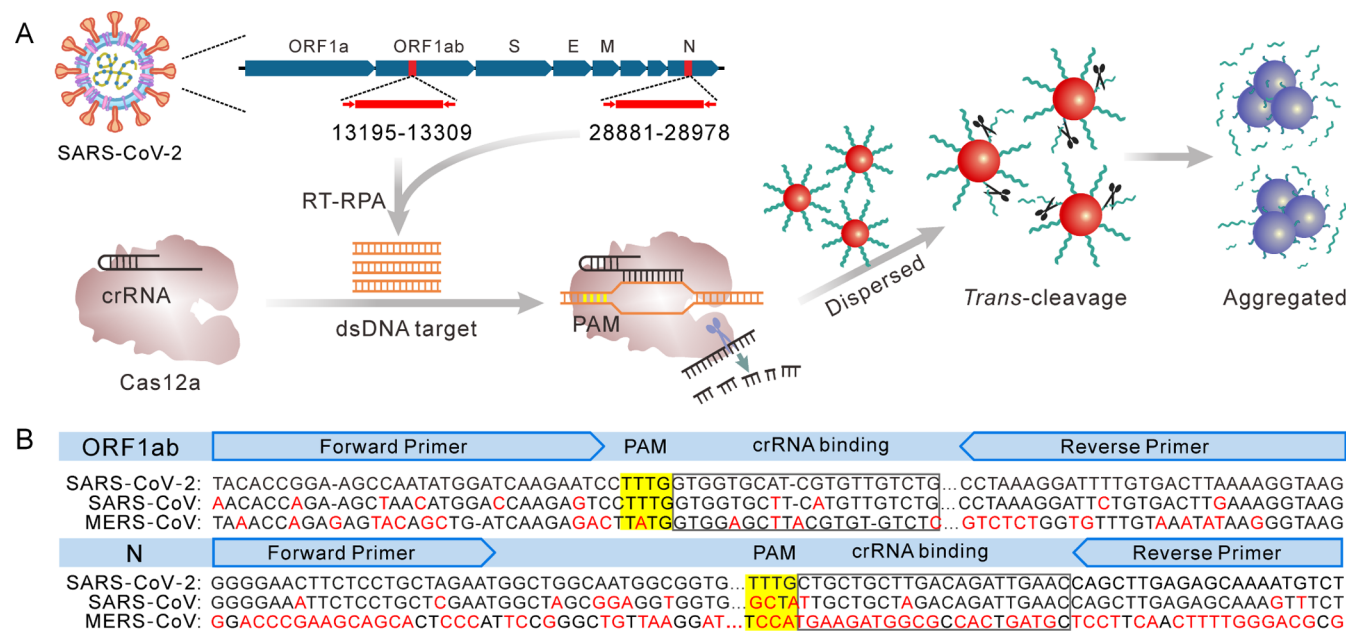
## ■ EXPERIMENTAL SECTION

**Reagents and Apparatus.** Oligonucleotides were designed with the help of Integrated DNA Technology and bought from Sangon Biotech Co., Ltd (Shanghai, China). Sequences of oligonucleotides used in this work are listed in Table S1. The TwistAmp Basic kit for RPA was purchased from TwistDx Limited (UK). Cas12a and ProtoScript II Reverse Transcriptase were purchased from New England Biolabs (Beijing). Chloroauric acid (HAuCl<sub>4</sub>·3H<sub>2</sub>O) and sodium citrate for AuNPs synthesis were obtained from Aladdin (Shanghai). 6-Mercapto-1-hexanol (MCH) was purchased from J&K Scientific (Beijing). The RNase inhibitor was obtained from Beyotime Biotechnology (Shanghai). Ultrapure water with 18.2 MΩ·cm was used throughout the study. All reagents were used as received without further purification. The colorimetric assays were conducted in 1×NEBuffer 2.1 (New England Biolabs, Beijing) unless otherwise stated.

A UV1800PC spectrophotometer (Shanghai, China) was used to quantify oligonucleotides and obtain the UV–vis absorption spectra. All DNA samples were annealed on an Applied Biosystems 96-well thermocycler. Native polyacrylamide gel electrophoresis (8% PAGE) of the DNA was conducted on a Tanon EPS300 electrophoresis apparatus and imaged with a Syngene gel imaging system under UV light. Transmission electron microscopy (TEM) was carried out to observe the AuNPs using a JEM-1011 microscope (Japan) operating at the voltage of 100 kV.

**Construction of AuNP Probes.** The AuNPs employed herein were ~15 nm in diameter. The thiolated ssDNA was modified onto the AuNP surface through sulfur–gold bonds. AuNPs were synthesized according to the literature.<sup>44</sup> Briefly, 100 mg of HAuCl<sub>4</sub>·3H<sub>2</sub>O dissolved in 300 mL water was boiled before 264 mg sodium citrate in 30 mL water was added. The solution was stirred for 10 min while boiling. After cooling down to room temperature, AuNPs with a diameter of ~15 nm were obtained. Then, the AuNP concentration was adjusted to 5 nM according to the UV–vis absorption. The ssDNA was attached to the AuNP surface with a molar ratio of 400:1. 20 μL of the ssDNA substrate (100 μM) and 2 μL of TCEP (30 mM) were added to 78 μL of DEPC water to make a final volume of 100 μL. After incubation for 20 min, the

**Scheme 1. RT-RPA-Coupled Cas12a for Colorimetric Detection of SARS-CoV-2;** (A) Schematic Illustration of the Strategy Design; The Whole Process Consists of Three Steps: RT-RPA of the Selected SARS-CoV-2 Genome Region, Cas12a Activation and Colorimetric Detection; (B) SARS-CoV-2 Genome Alignment of the Selected Target Region in the ORF1ab Gene and the N Protein gene; The Accession Numbers of SARS-CoV-2, SARS-CoV, and MERS-CoV Genomes Were NC\_045512.2, AY278741.1, and NC\_019843.3, Respectively



abovementioned solution was mixed with 1 mL of AuNPs (5 nM). 10  $\mu$ L of Tween 20 (20%) was added to avoid the AuNP aggregation. The abovementioned mixture was stirred gently at room temperature for 12 h, during which 8 times of NaCl solution (0.05 M for the first two times and 0.1 M for the rest times) was added with an interval of 40 min. Subsequently, the reaction solution was slowly stirred for 24 h before centrifuged at 16000g for 15 min to remove the unconjugated nucleic acids. The as-prepared AuNP probes were obtained after washing two times with PBS and stored at 4  $^{\circ}$ C before use.

For MCH treating, the prepared AuNPs probes mentioned above were mixed with MCH (10  $\mu$ M). After 30 min incubation, the mixture solution was centrifuged at 16000g for 30 min. After washing 3 times with PBS, the AuNP probe with MCH treatment was obtained.

#### CRISPR-Cas12a System-Mediated Colorimetric Assay.

To perform the colorimetric assay, 4  $\mu$ L of Cas12a and 8  $\mu$ L of crRNA were added to 100  $\mu$ L 1 $\times$ NEBuffer 2.1 to get a final concentration of 20 and 40 nM, respectively. After incubation for 10 min at 37  $^{\circ}$ C, the target sequence from RPA or RT-RPA was added, followed by addition of 80  $\mu$ L as-prepared AuNPs. At the setting time point, the UV-vis absorption spectrum or naked eye observation was conducted.

**RPA Process to Amplify the Target Sequence.** For the cDNA amplification, 2.4  $\mu$ L of forward and reverse primers (10  $\mu$ M each) were added to the RPA TwistAmp Basic kit according to the operating instructions. Then, 13.2  $\mu$ L of target solution was mixed. At last, 2.5  $\mu$ L of MgOAc (280 mM) was added to initiate the amplification. After incubation for 20 min at 37  $^{\circ}$ C, the obtained RPA products were stored at 4  $^{\circ}$ C before use.

**Clinical Standard Sample Analysis.** RT-RPA was employed to amplify the target sequence in the clinical standard sample. 2.4  $\mu$ L of forward primer (10  $\mu$ M), 2.4  $\mu$ L of reverse primer (10  $\mu$ M), and 1  $\mu$ L of RNA reverse

transcriptase together with 10  $\mu$ L of RNase inhibitor were added to the RPA TwistAmp Basic kit. After addition of the clinical sample, the mixed solution was incubated for 20 min at 37  $^{\circ}$ C. The obtained dsDNA products were stored at 4  $^{\circ}$ C before being used for colorimetric assay.

## RESULTS AND DISCUSSION

### RT-RPA-Coupled CRISPR-Cas12a Colorimetric Assay for SARS-CoV-2 Detection.

An assay strategy of selective targeting and sensitive detection of the aiming gene sequence of SARS-CoV-2 without access to sophisticated instruments would greatly benefit COVID-19 diagnosis. Cas12a exhibited a specific cleavage activity toward bound DNA (*cis*-cleavage) with a sequence complementary to the crRNA and subsequent indiscriminate ssDNA hydrolysis (*trans*-cleavage). Once activated by the target sequence, the collateral cleavage of the ssDNA substrate can reach as high as  $\sim$ 1250 turnovers per second.<sup>45</sup> Meanwhile, the RT-RPA process will reverse-transcribe and amplify the RNA genome sequence in a short time under an isothermal condition. Through integration of the RT-RPA-coupled Cas12a system with optical properties of AuNPs, we developed a novel colorimetric SARS-CoV-2 genome detection platform (Scheme 1A). In the method proposed herein, AuNPs, capped with thiolated ssDNA, acted as a universal substrate for Cas12a cleavage. In the absence of the SARS-CoV-2 genome, Cas12a stayed inactive and AuNPs remained in a well-dispersed state. When the virus genome was amplified through RT-RPA, the resulting abundant dsDNA will undergo crRNA-guided binding to activate Cas12a. Under *trans*-cleavage degradation, the capped ssDNA strands were hydrolyzed gradually and AuNPs aggregated, demonstrating a change in their SPR. The overall detection was operated in homogeneous medium without any separation or heating cycle process and significantly increased the feasibility for COVID-19 detection.

**Target Mapping and Primer Design.** As an RNA virus, the molecular diagnosis of SARS-CoV-2 primarily relied on the detection of species-specific gene regions. The gene encoding for E, N, S, and ORF1ab protein has been selected by countries worldwide. For instance, Chinese CDC chose the ORF1ab and N gene as target sites for COVID-19 clinic diagnosis, while US CDC utilized two sites located in the N region.<sup>46</sup> To achieve direct comparison between our method and the established Chinese clinical test assay, we designed the primers for RT-RPA and crRNA for Cas12a targeting the ORF1ab and N regions, respectively. Both the regions selected contained a protospacer adjacent motif (PAM) required for Cas12a activation. The sequence alignment of selected SARS-CoV-2 regions with corresponding sites of other beta coronaviruses (SARS-CoV and MERS-CoV) is illustrated in Scheme 1B. There were overall four functional regions along the target sequence: a forward primer, PAM, crRNA binding region, and reverse primer. The RT-RPA efficiency was determined by the forward and reverse primer regions, while the PAM recognition and crRNA binding were indispensable for Cas12a activation.

The variations located in the ORF1ab regions of SARS-CoV and MERS-CoV (marked in red in Scheme 1B) were in different degrees of correlation with target regions. For the ORF1ab gene, more difference was observed for MERS-CoV, which showed over four variations in each functional region. In terms of SARS-CoV, variations are less, which is in agreement with the relative phylogenetic distance.<sup>47</sup> There were five variations for SARS-CoV in the forward primer region, while two variations in both crRNA binding and reverse primer region. As for the N gene region, MERS-CoV did not show any significant similarity to the selected SARS-CoV-2 target, while SARS-CoV showed significant agreement in primer and crRNA binding regions. Notably, the three variations among the four PAM nucleotides will efficiently reduce the recognition probability to Cas12a.<sup>25</sup> The impacted RT-RPA efficiency due to mismatches of primers together with the inhibited Cas12a cleavage ability from an inefficient crRNA binding guaranteed the specificity of our method, decreasing the likelihood of a false positive readout caused by SARS-CoV and MERS-CoV.

**Verification and Characterization of the Proposed Colorimetric Assay.** In our design, the target sequence was first amplified through RT-RPA, and then it yielded a colorimetric readout through Cas12a-mediated trans-cleavage of the AuNP probes. As a proof of concept, the corresponding cDNA of the selected ORF1ab and N regions were chosen and the RPA results were analyzed through PAGE. We can conclude that the cDNA for both regions can be efficiently amplified within 20 min in a dose-dependent manner (Figure S1). Then, we utilized PAGE (Figure 1A) to characterize the feasibility of Cas12a trans-cleavage property. As per our hypothesis, the cleavage occurred only in the presence of both dsDNA target and crRNA (lane 5 in Figure 1A). The AuNP probes utilized herein were functionalized with thiolated ssDNA according to the method reported previously.<sup>48</sup> TEM images showed that the modified AuNPs were in an individually dispersed state with the core diameter of ~15 nm and exhibited good stability, maintaining 99% of the optical absorption after 1 week storage (Figure S2). Then, we tested the detection feasibility of Cas12a-mediated colorimetric assay with the UV-vis spectrum, and the procedure is illustrated in Figure 1B. In our design, after activation by target DNA, Cas12a will degrade the ssDNA from the AuNP

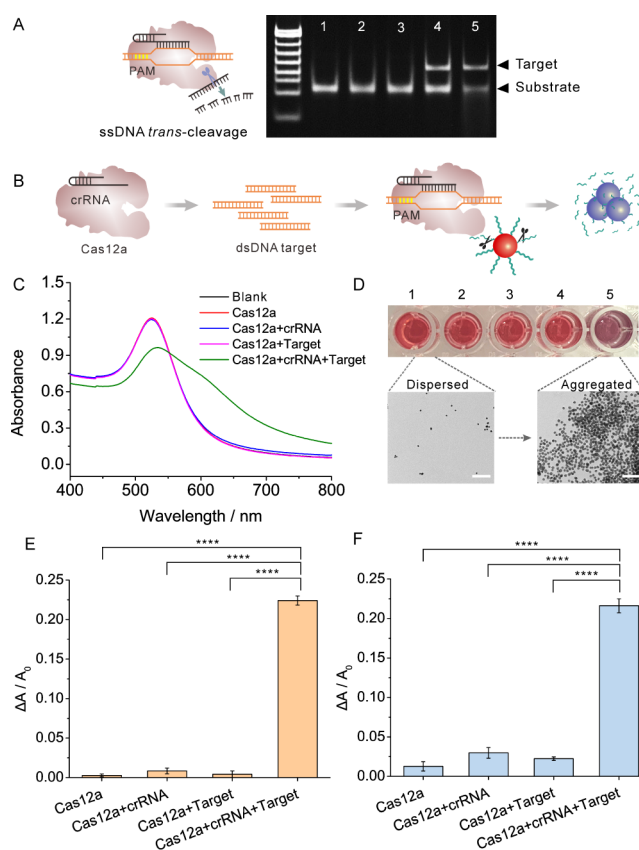


**Figure 1.** Feasibility verification of Cas12a-mediated colorimetric detection. (A) PAGE analysis of the ssDNA trans-cleavage ability of Cas12a after activated by target strands. Lane 1: substrate; lane 2: substrate + Cas12a; lane 3: substrate + Cas12a + crRNA; lane 4: substrate + Cas12a + Target; lane 5: substrate + Cas12a + crRNA + Target. Incubation time: 15 min. [Cas12a]: 20 nM, [crRNA]: 40 nM, [Target]: 40 nM, [Substrate]: 1  $\mu$ M; loading volume: 10  $\mu$ L. Running at 80 V for 80 min. (B) Schematic illustration of the AuNP aggregation resulting from the trans-cleavage of Cas12a. After activation, the Cas12a will cut and release the nucleic acids from the AuNP surface, leading to AuNP aggregation. The distance-dependent optical properties of the AuNPs can be clearly recorded with UV-vis and observed with naked eyes. (C) UV-vis absorption spectra of AuNP probes in different reaction conditions. (D) Color change and TEM images of AuNP probes in different reaction conditions. Well 1: blank; well 2: Cas12a; well 3: Cas12a + crRNA; well 4: Cas12a + target; well 5: Cas12a + crRNA + target. Scale bar: 100 nm. The variations of the relative variation ratio of absorption at 520 nm for ORF1ab (E) and N (F) gene targets in different reaction conditions, respectively. Bar graph data represent mean  $\pm$  SD ( $n = 3$ ). (\*\*\*\*,  $P < 0.0001$ ).

surface, leading to a decreased and red-shifted SPR peak along with AuNP aggregation. As shown in Figure 1C, the buffer containing AuNP probes displayed an SPR peak at 520 nm. The addition of a preincubated Cas12a/crRNA complex did not make any difference to the absorption curve. In contrast, the addition of an RPA target along with the Cas12a/crRNA induced obvious absorption reduction as well as red shift of the SPR peak. Concomitantly, we also observed the color change in the abovementioned different reaction conditions. In Figure 1D, the reaction color in well 5 turned from red to purple, where the target was added along with the Cas12a/crRNA complex. The color change can be ascribed to the aggregation of AuNPs, as exhibited in the TEM image in Figure 1D.<sup>29,49</sup>

The variations of relative variation ratio of absorption at 520 nm ( $\Delta A/A_0$ ) were analyzed, as shown in Figure 1E, which demonstrated that SPR change caused by the target sequence could be used to perform the ORF1ab detection assays. Next, the feasibility for cDNA from the N region was also investigated in the same way, just by changing the primer pair and crRNA accordingly. As shown in Figure 1F, only the presence of an N region target sequence and Cas12a/crRNA complex can yield significantly improved  $\Delta A/A_0$ . All these results confirmed the feasibility of our isothermal amplification-coupled Cas12a-based colorimetric assay for SARS-CoV-2 detection.

**Optimization of the Detection Conditions.** Prior to exploitation of our proposed method for SARS-CoV-2 genome detection, several critical parameters have been optimized to achieve the best performance. The thiol-terminated ssDNAs function as AuNP stabilizing agents as well as Cas12a substrates simultaneously. Thus, the length of the ssDNA may play a significant role in our method. We increased the ssDNA length from 20 to 70 nt and found that the performances did not show a significant difference among these ssDNA (Figure 2A). Accordingly, the MCH capping

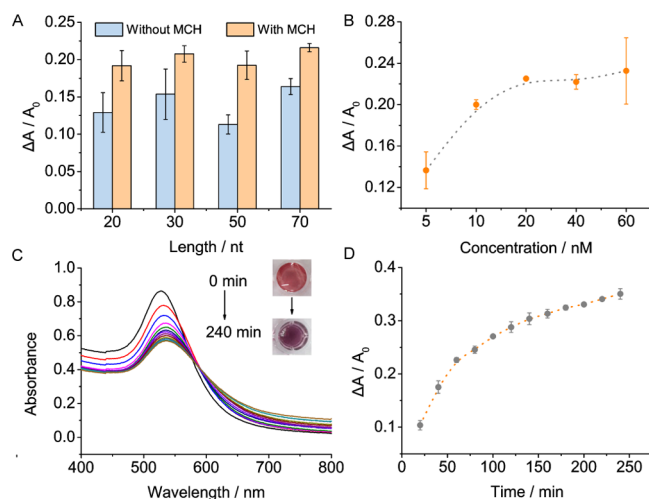


**Figure 2.** Optimization of the detection conditions. (A) Influences of MCH treatment and substrate length to the colorimetric assays. The UV-vis absorption spectra were obtained after 1 h of reaction. 4  $\mu\text{L}$  of Cas12a (1  $\mu\text{M}$ ) and 8  $\mu\text{L}$  of crRNA (1  $\mu\text{M}$ ) were pre-incubated for 10 min before they were mixed with 8  $\mu\text{L}$  of target (ORF1ab segments, 1  $\mu\text{M}$ ) in a 100  $\mu\text{L}$  reaction system including 80  $\mu\text{L}$  AuNP probes. (B) Concentration-dependent effect of Cas12a/crRNA on the readout signals. (C) and (D) Reaction time optimization. UV-vis absorption spectra were recorded at an interval of 20 min. The error bars represented the standard deviations of three repetitive experiments.

effect was also investigated. MCH can displace the noncovalent base adsorption on the surface as well as change the oligonucleotide conformation, which will facilitate the accessibility of Cas12a.<sup>50</sup> In Figure 2A, we can observe a similar tendency but with higher relative variation ratios after MCH treatment for different ssDNA lengths. As the 20 nt capping AuNPs were less stable, considering the detection cost, we selected 30 nt ssDNA with an MCH capping method for AuNP preparation.

The target dsDNA recognition is a prerequisite for trans-cleavage of Cas12a. After crRNA-guided target recognition,

ssDNA substrates can be degraded rapidly from the RuvC domain with a catalytic efficiency approaching the rate of diffusion. As the Cas12a/gRNA-bound dsDNA target with a stoichiometric ratio of 1:1, we anticipate that more Cas12a/crRNA complexes will render faster colorimetric reaction kinetics. By fixing the target sequence at 40 nM, we investigated the concentration of the Cas12a/crRNA complex ranging from 5 to 60 nM. Figure 2B illustrates an increase in the relative absorption variation ratio until 20 nM, and the performance reached a plateau with higher concentrations. Therefore, the 20 nM Cas12a/crRNA complex was utilized for further investigation.

In our design, AuNP probes will undergo aggregation under the stochastic trans-cleavage process. More incubation time will lead to more ssDNA degradation. Hence, the trans-cleavage time of Cas12a was further analyzed. After target addition, with the solution turned from red to purple, the absorption at 520 nm decreased accordingly (Figure 2C). The  $\Delta A/A_0$  analysis shown in Figure 2D revealed that the reaction kinetics become slower after 60 min. As the reaction proceeded, fewer substrates made the accessibility of activated Cas12a harder, which may account for the decreased hydrolysis kinetics. Therefore, 60 min was chosen as the most suitable reaction time. Notably, the reaction time can be further shortened to within 30 min with the assistance of low-speed centrifugation. We investigated the working efficiency by monitoring the  $\Delta A/A_0$  for different reaction times (10–30 min) before centrifugation (5000 rpm, 3 min). According to the results in Figure S3, higher reaction time will yield a higher detection signal, and 30 min was long enough to get the same performance as 60 min without centrifugation. Moreover, the low-speed centrifugation method was able to achieve a significant difference with blank control just with 10 min reaction, which made a more efficient alternative for those laboratories equipped with centrifuges.

#### Detection Performance of the Colorimetric Assay.

Under the optimized experimental conditions, the performance of our proposed colorimetric assay was studied against a series of different concentrations of targets from the ORF1ab region. As shown in Figure S4, the UV-vis absorption at 520 nm decreased accordingly with the increase of target concentrations, which was consistent with the color change of the reaction solution (Figure 3A). Then, the correlation of the relative variation ratio with target concentration was studied. A good linearity can be obtained ranging from 10 pM to 100 nM (Figure 3A, inset). Owing to the Cas12a-mediated catalysis, the great sensitivity of our method exhibits huge potential for COVID-19 diagnosis when accommodated with the RT-RPA pre-amplification process.

Then, we attempted to investigate the specificity of our method by challenging the two other beta coronaviruses, SARS-CoV and MERS-CoV, which had  $\sim 82$  and  $\sim 67\%$  similarity to the genome of the SARS-CoV-2, respectively.<sup>47</sup> The sequence alignment of these three genome regions was illustrated and analyzed, as shown in Scheme 1B. The selected ORF1ab cDNA segments were amplified by RPA and then analyzed with the Cas12a-mediated colorimetric assay, as exhibited in Figure 3B. The  $\Delta A/A_0$  for SARS-CoV and MERS-CoV in Figure 3C were significantly lower than SARS-CoV-2. Although the unexpected amplification or primer dimer interference is inevitable for RPA, the RPA products will undergo a second checking process during crRNA-mediated binding and activation of Cas12a. The nonspecific amplifica-

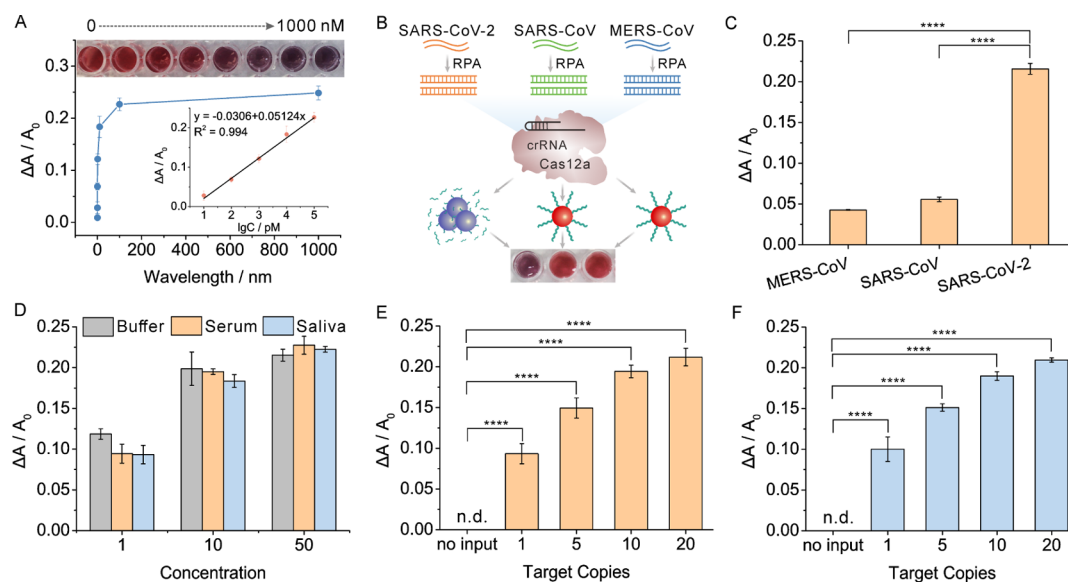


**Figure 3.** Colorimetric target detection based on Cas12a. (A) Correlation of relative variation ratios and color change image with different concentrations of target strands (0, 0.001, 0.01, 0.1, 1, 10, 100, and 1000 nM). Inset: the linear relationship between the relative variation ratio and target concentrations. (B) Illustration of the detection procedure and the resulting color from different viruses. (C) Specificity of our method against SARS-CoV and MERS-CoV sequences in ORF1ab. All the target sequences used were 100 fM before RPA amplification. (D) Relative absorption variation ratios at 520 nm in reaction buffer, human serum, and saliva matrixes spiked with different amounts of target sequences. (E) and (F) Sensitivity test. Different numbers of the SARS-CoV-2 sequence in ORF1ab (E) and N gene (F) region were analyzed through Cas12a mediated colorimetric assay after amplification by RPA. Error bars represent the standard deviations of three repetitive experiments. (n.d., not detected; \*\*\*\*,  $P < 0.0001$ ).

tion products from primer dimer or other segments will be hardly recognized by crRNA or activated by Cas12a. The variations located in the primer region of SARS-CoV and MERS-CoV will impact the RPA efficiency. Meanwhile, the mismatches in PAM- and crRNA-binding regions inhibited Cas12a recognition and cleavage ability. The synergistic effect from RPA and Cas12a decreased the likelihood of false positive events and increased the specificity of our method proposed herein.

To meet the requirement for clinical diagnosis, the performance robustness in complex biosamples is of vital importance. Thus, our detection method was carried out with the interference from spiked serum and saliva samples, both of which were the common matrixes for SARS-CoV-2 clinical samples. Typically, the biosample was spiked with different concentrations of SARS-CoV-2 target regions (ORF1ab). Then, the UV–vis spectra were measured. From the results in Figure 3D, we can infer that the signal readouts from the spiked biosamples did not show any significant difference to reaction buffer, especially for concentrations higher than 10 nM, indicating that our method holds great potential for complex biological samples analysis.

The inherent high amplification efficiency from RPA will generate plenty of target dsDNA copies for subsequent colorimetric detection. To investigate the detection sensitivity, different number of cDNA copies from the ORF1ab (115 nt) and N (98 nt) gene regions of SARS-CoV-2 genome were pre-amplified through RPA and then analyzed with the Cas12a-mediated colorimetric assay. As shown in Figure 3E,F, our method was capable of detecting as low as 1 copy of genome sequence for both ORF1ab and N gene regions, which was superior to the detection methods proposed recently for SARS-CoV-2 (Table S2). This high sensitivity (1 copy per test)

ensured that our method had great potential for COVID-19 diagnosis.

**Clinical Standard Sample Analysis with the RT-RPA-Coupled Cas12a Colorimetric Detection.** For the analysis of clinical samples, standard positive and negative samples of SARS-CoV-2 from the clinical laboratory department were tested. As the genetic material in positive standard control was RNA, RT-RPA was conducted to reverse-transcribe the target RNA into cDNA before amplification to dsDNA (Figure 4A).

PAGE shown in Figure S5 verified the successful amplification of ORF1ab and N gene segments in the positive RNA sample to dsDNA products by RT-RPA. The subsequent

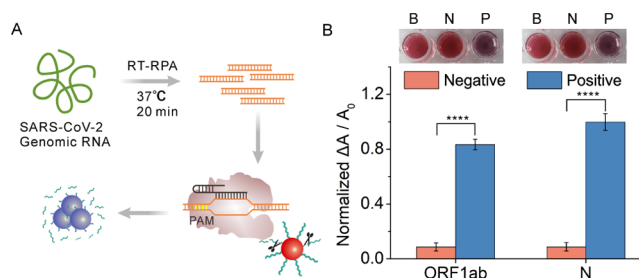


**Figure 4.** Clinical standard sample analysis. (A) Schematic illustration of the RT-RPA-coupled Cas12a colorimetric assay for clinical SARS-CoV-2 genome samples. The RNA sample was reverse-transcribed to cDNA before being amplified through RPA. The resulting dsDNA target bound and activated the Cas12a trans-cleavage ability. The dispersed AuNP probes will turn into aggregation states after the cleavage of the capped ssDNA. (B) Relative absorption variation ratios at 520 nm of negative and positive clinical standard samples provided by the hospital laboratory department. The error bars represented the standard deviations of three repetitive experiments. B: blank control, N: negative sample, P: positive sample. (\*\*\*\*,  $P < 0.0001$ ).

Cas12a-mediated colorimetric results exhibited complete concordance with the intrinsic sample property for both ORF1ab and N gene regions (Figure 4B), demonstrating great reliability of our method for practical COVID-19 diagnosis in clinic. Notably, the positive results can be clearly observed through color change of the solution by naked eyes, making the RT-RPA-coupled Cas12a colorimetric assay a simple-yet-effective diagnosis candidate. We also verified the feasibility of the low-speed centrifugation method proposed above for clinical sample analysis (Figure S6). With the assistance of centrifugation, the total reaction could be finished within 1 h (20 min for isothermal amplification and 30 min for colorimetric readout), which may endow greater potential for practical diagnosis.

## CONCLUSIONS

In summary, RT-RPA-coupled CRISPR-Cas12a colorimetric assay was proposed in this work for SARS-CoV-2 genome detection. This method exhibited exclusive features for potential SARS-CoV-2 detection: (a) the interparticle distance-dependent plasmon of AuNPs made a facial and international colorimetric readout for different target sequences; (b) the synergistic variation checking effect from RT-RPA and Cas12a significantly decreased the likelihood of false positive events and increased the specificity; (c) the amplification from RT-RPA and Cas12a trans-cleavage process bring the sensitivity of our method to 1 copy of viral genome sequence per test, ensuring our method had great potential for sensitive COVID-19 diagnosis; (d) the reliability of this colorimetric assay was validated by standard clinical samples from the hospital laboratory department. While the existing detection techniques remain laborious and technically challenging, the colorimetric assay proposed herein can be carried out without thermal cycles or sophisticated instruments. Through integration of the inherently high sensitivity and specificity from the RT-RPA-coupled Cas12a system with the simplicity of AuNP-based colorimetric assay, our method, which can provide fast and facial test results, was a promising candidate for simple-yet-effective diagnosis for COVID-19.

## ASSOCIATED CONTENT

### Supporting Information

The Supporting Information is available free of charge at <https://pubs.acs.org/doi/10.1021/acs.analchem.1c00013>.

TEM image and stability analysis of synthesized AuNPs; detection performance for different reaction time with the low-speed centrifugation method; UV-vis absorption spectra of target strands; PAGE results and low-speed centrifugation method results for the clinical standard samples; and all the oligonucleotides used in this work and comparison of the detection performance (PDF)

## AUTHOR INFORMATION

### Corresponding Authors

**Yanyan Yu** – School of Pharmacy, Nantong University, Nantong, Jiangsu 226001, China; [orcid.org/0000-0002-5806-0896](https://orcid.org/0000-0002-5806-0896); Email: [yuyanyan@ntu.edu.cn](mailto:yuyanyan@ntu.edu.cn)

**Gaoxing Su** – School of Pharmacy, Nantong University, Nantong, Jiangsu 226001, China; [orcid.org/0000-0001-9607-2006](https://orcid.org/0000-0001-9607-2006); Email: [sugaoxing@ntu.edu.cn](mailto:sugaoxing@ntu.edu.cn)

## Authors

**Wei S. Zhang** – School of Pharmacy, Nantong University, Nantong, Jiangsu 226001, China

**Jianbin Pan** – State Key Laboratory of Analytical Chemistry for Life Science, School of Chemistry and Chemical Engineering, Nanjing University, Nanjing, Jiangsu 210093, China

**Feng Li** – Affiliated Hospital of Nantong University, Nantong, Jiangsu 226001, China

**Min Zhu** – School of Pharmacy, Nantong University, Nantong, Jiangsu 226001, China

**Mengting Xu** – School of Pharmacy, Nantong University, Nantong, Jiangsu 226001, China

**Hongyan Zhu** – School of Pharmacy, Nantong University, Nantong, Jiangsu 226001, China; [orcid.org/0000-0002-5985-8533](https://orcid.org/0000-0002-5985-8533)

Complete contact information is available at:

<https://pubs.acs.org/10.1021/acs.analchem.1c00013>

## Author Contributions

<sup>||</sup>W.S.Z. and J.P. contribute equally to this work.

## Notes

The authors declare no competing financial interest.

## ACKNOWLEDGMENTS

This study was supported by the National Natural Science Foundation of China (grants 21705082), the Natural Science Foundation of Jiangsu Province in China (BK20170444), State Key Laboratory of Analytical Chemistry for Life Science (SKLACLS2013), the Science and Technology Plan Projects of Nantong (XG202008-4), and Large Instruments Open Foundation of Nantong University (KFJN2059).

## REFERENCES

- (1) Zhou, P.; Yang, X.-L.; Wang, X.-G.; Hu, B.; Zhang, L.; Zhang, W.; Si, H.-R.; Zhu, Y.; Li, B.; Huang, C.-L.; Chen, H.-D.; Chen, J.; Luo, Y.; Guo, H.; Jiang, R.-D.; Liu, M.-Q.; Chen, Y.; Shen, X.-R.; Wang, X.; Zheng, X.-S.; et al. *Nature* **2020**, *579*, 270–273.
- (2) Wu, F.; Zhao, S.; Yu, B.; Chen, Y.-M.; Wang, W.; Song, Z.-G.; Hu, Y.; Tao, Z.-W.; Tian, J.-H.; Pei, Y.-Y.; Yuan, M.-L.; Zhang, Y.-L.; Dai, F.-H.; Liu, Y.; Wang, Q.-M.; Zheng, J.-J.; Xu, L.; Holmes, E. C.; Zhang, Y.-Z. *Nature* **2020**, *579*, 265–269.
- (3) Zhu, N.; Zhang, D.; Wang, W.; Li, X.; Yang, B.; Song, J.; Zhao, X.; Huang, B.; Shi, W.; Lu, R.; Niu, P.; Zhan, F.; Ma, X.; Wang, D.; Xu, W.; Wu, G.; Gao, G. F.; Tan, W. *N. Engl. J. Med.* **2020**, *382*, 727–733.
- (4) Liu, Y.; Gayle, A. A.; Wilder-Smith, A.; Rocklöv, J. *J. Travel Med.* **2020**, *27*, taaa021.
- (5) Chauhan, G.; Madou, M. J.; Kalra, S.; Chopra, V.; Ghosh, D.; Martinez-Chapa, S. O. *ACS Nano* **2020**, *14*, 7760–7782.
- (6) Udugama, B.; Kadhiresan, P.; Kozłowski, H. N.; Malekjahani, A.; Osborne, M.; Li, V. Y. C.; Chen, H.; Mubareka, S.; Gubbay, J. B.; Chan, W. C. W. *ACS Nano* **2020**, *14*, 3822–3835.
- (7) Chan, J. F.-W.; Yip, C. C.-Y.; To, K. K.-W.; Tang, T. H.-C.; Wong, S. C.-Y.; Leung, K.-H.; Fung, A. Y.-F.; Ng, A. C.-K.; Zou, Z.; Tsoi, H.-W.; Choi, G. K.-Y.; Tam, A. R.; Cheng, V. C.-C.; Chan, K.-H.; Tsang, O. T.-Y.; Yuen, K.-Y. *J. Clin. Microbiol.* **2020**, *58*, e00310–e00320.
- (8) Chu, D. K. W.; Pan, Y.; Cheng, S. M. S.; Hui, K. P. Y.; Krishnan, P.; Liu, Y.; Ng, D. Y. M.; Wan, C. K. C.; Yang, P.; Wang, Q.; Peiris, M.; Poon, L. L. M. *Clin. Chem.* **2020**, *66*, 549–555.
- (9) Feng, W.; Newbigging, A. M.; Le, C.; Pang, B.; Peng, H.; Cao, Y.; Wu, J.; Abbas, G.; Song, J.; Wang, D.-B.; Cui, M.; Tao, J.; Tyrrell, D. L.; Zhang, X.-E.; Zhang, H.; Le, X. C. *Anal. Chem.* **2020**, *92*, 10196–10209.

- (10) Chan, W. C. W. *ACS Nano* **2020**, *14*, 3719–3720.
- (11) Bhalla, N.; Pan, Y.; Yang, Z.; Payam, A. F. *ACS Nano* **2020**, *14*, 7783–7807.
- (12) Zhao, Y.; Chen, F.; Li, Q.; Wang, L.; Fan, C. *Chem. Rev.* **2015**, *115*, 12491–12545.
- (13) Rabe, B. A.; Cepko, C. *Proc. Natl. Acad. Sci. U.S.A.* **2020**, *117*, 24450–24458.
- (14) Notomi, T.; Okayama, H.; Masubuchi, H.; Yonekawa, T.; Watanabe, K.; Amino, N.; Hase, T. *Nucleic Acids Res.* **2000**, *28*, No. e63.
- (15) Huang, Z.; Tian, D.; Liu, Y.; Lin, Z.; Lyon, C. J.; Lai, W.; Fusco, D.; Drouin, A.; Yin, X.; Hu, T.; Ning, B. *Biosens. Bioelectron.* **2020**, *164*, 112316.
- (16) Li, Y.; Li, S.; Wang, J.; Liu, G. *Trends Biotechnol.* **2019**, *37*, 730–743.
- (17) Xiong, Y.; Zhang, J.; Yang, Z.; Mou, Q.; Ma, Y.; Xiong, Y.; Lu, Y. *J. Am. Chem. Soc.* **2020**, *142*, 207–213.
- (18) Chertow, D. S. *Science* **2018**, *360*, 381–382.
- (19) Qin, P.; Park, M.; Alfson, K. J.; Tamhankar, M.; Carrion, R.; Patterson, J. L.; Griffiths, A.; He, Q.; Yildiz, A.; Mathies, R.; Du, K. *ACS Sens.* **2019**, *4*, 1048–1054.
- (20) Broughton, J. P.; Deng, X.; Yu, G.; Fasching, C. L.; Servellita, V.; Singh, J.; Miao, X.; Streithorst, J. A.; Granados, A.; Sotomayor-Gonzalez, A.; Zorn, K.; Gopez, A.; Hsu, E.; Gu, W.; Miller, S.; Pan, C.-Y.; Guevara, H.; Wadford, D. A.; Chen, J. S.; Chiu, C. Y. *Nat. Biotechnol.* **2020**, *38*, 870–874.
- (21) Gootenberg, J. S.; Abudayyeh, O. O.; Lee, J. W.; Essletzbichler, P.; Dy, A. J.; Joung, J.; Verdine, V.; Donghia, N.; Daringer, N. M.; Freije, C. A.; Myhrvold, C.; Bhattacharyya, R. P.; Livny, J.; Regev, A.; Koonin, E. V.; Hung, D. T.; Sabeti, P. C.; Collins, J. J.; Zhang, F. *Science* **2017**, *356*, 438.
- (22) Zhang, F.; Abudayyeh, O. O.; Gootenberg, J. S. A Protocol for Detection of COVID-19 Using CRISPR Diagnostics. 2020, [https://www.broadinstitute.org/files/publications/special/COVID-19%20detection%20\(updated\).pdf](https://www.broadinstitute.org/files/publications/special/COVID-19%20detection%20(updated).pdf) (accessed 2020-05-11).
- (23) Gootenberg, J. S.; Abudayyeh, O. O.; Kellner, M. J.; Joung, J.; Collins, J. J.; Zhang, F. *Science* **2018**, *360*, 439–444.
- (24) Myhrvold, C.; Freije, C. A.; Gootenberg, J. S.; Abudayyeh, O. O.; Metsky, H. C.; Durbin, A. F.; Kellner, M. J.; Tan, A. L.; Paul, L. M.; Parham, L. A.; Garcia, K. F.; Barnes, K. G.; Chak, B.; Mondini, A.; Nogueira, M. L.; Isern, S.; Michael, S. F.; Lorenzana, I.; Yozwiak, N. L.; MacInnis, B. L.; et al. *Science* **2018**, *360*, 444–448.
- (25) Chen, J. S.; Ma, E.; Harrington, L. B.; Da Costa, M.; Tian, X.; Palefsky, J. M.; Doudna, J. A. *Science* **2018**, *360*, 436.
- (26) Liu, J.-J.; Orlova, N.; Oakes, B. L.; Ma, E.; Spinner, H. B.; Baney, K. L. M.; Chuck, J.; Tan, D.; Knott, G. J.; Harrington, L. B.; Al-Shayeb, B.; Wagner, A.; Brötzmann, J.; Staahl, B. T.; Taylor, K. L.; Desmarais, J.; Nogales, E.; Doudna, J. A. *Nature* **2019**, *566*, 218–223.
- (27) English, M. A.; Soenksen, L. R.; Gayet, R. V.; de Puig, H.; Angenent-Mari, N. M.; Mao, A. S.; Nguyen, P. Q.; Collins, J. J. *Science* **2019**, *365*, 780–785.
- (28) Moitra, P.; Alafeef, M.; Dighe, K.; Frieman, M. B.; Pan, D. *ACS Nano* **2020**, *14*, 7617–7627.
- (29) Li, H.; Rothberg, L. J. *J. Am. Chem. Soc.* **2004**, *126*, 10958–10961.
- (30) Li, H.; Rothberg, L. *Proc. Natl. Acad. Sci. U.S.A.* **2004**, *101*, 14036.
- (31) Yang, H.; Xiao, M.; Lai, W.; Wan, Y.; Li, L.; Pei, H. *Anal. Chem.* **2020**, *92*, 4990–4995.
- (32) Man, T.; Ji, W.; Liu, X.; Zhang, C.; Li, L.; Pei, H.; Fan, C. *ACS Nano* **2019**, *13*, 4826–4833.
- (33) Saha, K.; Agasti, S. S.; Kim, C.; Li, X.; Rotello, V. M. *Chem. Rev.* **2012**, *112*, 2739–2779.
- (34) Zhou, W.; Gao, X.; Liu, D.; Chen, X. *Chem. Rev.* **2015**, *115*, 10575–10636.
- (35) Li, Z.; Askim, J. R.; Suslick, K. S. *Chem. Rev.* **2019**, *119*, 231–292.
- (36) Baetsen-Young, A. M.; Vasher, M.; Matta, L. L.; Colgan, P.; Alocilja, E. C.; Day, B. *Biosens. Bioelectron.* **2018**, *101*, 29–36.
- (37) Elghanian, R.; Storhoff, J. J.; Mucic, R. C.; Letsinger, R. L.; Mirkin, C. A. *Science* **1997**, *277*, 1078–1081.
- (38) Cutler, J. I.; Auyeung, E.; Mirkin, C. A. *J. Am. Chem. Soc.* **2012**, *134*, 1376–1391.
- (39) Sperling, R. A.; Rivera Gil, P.; Zhang, F.; Zanella, M.; Parak, W. *J. Chem. Soc. Rev.* **2008**, *37*, 1896–1908.
- (40) Hu, M.; Yuan, C.; Tian, T.; Wang, X.; Sun, J.; Xiong, E.; Zhou, X. *J. Am. Chem. Soc.* **2020**, *142*, 7506–7513.
- (41) Yuan, C.; Tian, T.; Sun, J.; Hu, M.; Wang, X.; Xiong, E.; Cheng, M.; Bao, Y.; Lin, W.; Jiang, J.; Yang, C.; Chen, Q.; Zhang, H.; Wang, H.; Wang, X.; Deng, X.; Liao, X.; Liu, Y.; Wang, Z.; Zhang, G.; et al. *Anal. Chem.* **2020**, *92*, 4029–4037.
- (42) Pan, D.; Pramanik, M.; Senpan, A.; Yang, X.; Song, K. H.; Scott, M. J.; Zhang, H.; Gaffney, P. J.; Wickline, S. A.; Wang, L. V.; Lanza, G. M. *Angew. Chem., Int. Ed.* **2009**, *48*, 4170–4173.
- (43) Misra, S. K.; Dighe, K.; Schwartz-Duval, A. S.; Shang, Z.; Labriola, L. T.; Pan, D. *Biosens. Bioelectron.* **2018**, *120*, 77–84.
- (44) Giljohann, D. A.; Seferos, D. S.; Patel, P. C.; Millstone, J. E.; Rosi, N. L.; Mirkin, C. A. *Nano Lett.* **2007**, *7*, 3818–3821.
- (45) Liang, M.; Li, Z.; Wang, W.; Liu, J.; Liu, L.; Zhu, G.; Karthik, L.; Wang, M.; Wang, K. F.; Wang, Z.; Yu, J.; Shuai, Y.; Yu, J.; Zhang, L.; Yang, Z.; Li, C.; Zhang, Q.; Shi, T.; Zhou, L.; Xie, F.; et al. *Nat. Commun.* **2019**, *10*, 3672.
- (46) Ji, T.; Liu, Z.; Wang, G.; Guo, X.; Akbar Khan, S.; Lai, C.; Chen, H.; Huang, S.; Xia, S.; Chen, B.; Jia, H.; Chen, Y.; Zhou, Q. *Biosens. Bioelectron.* **2020**, *166*, 112455.
- (47) Naqvi, A. A. T.; Fatima, K.; Mohammad, T.; Fatima, U.; Singh, I. K.; Singh, A.; Atif, S. M.; Hariprasad, G.; Hasan, G. M.; Hassan, M. I. *BBA, Mol. Basis Dis.* **2020**, *1866*, 165878.
- (48) Yu, Y.; Zhang, W. S.; Guo, Y.; Peng, H.; Zhu, M.; Miao, D.; Su, G. *Biosens. Bioelectron.* **2020**, *167*, 112482.
- (49) Yoo, S. M.; Lee, S. Y. *Trends Biotechnol.* **2016**, *34*, 7–25.
- (50) Park, S.; Brown, K. A.; Hamad-Schifferli, K. *Nano Lett.* **2004**, *4*, 1925–1929.